

Influence of Surface Temperature and Emissivity on AMSU-A Assimilation over Land*

HE Wenying^{1†}(何文英), LIU Zhiquan²(刘志权), and CHEN Hongbin¹(陈洪滨)

¹ LAGEO, Institute of Atmospheric Physics, Chinese Academy of Sciences, Beijing 100029, China

² National Center for Atmospheric Research (NCAR) Earth System Laboratory, Boulder, Colorado 80305, USA

(Received October 4, 2010; in final form March 25, 2011)

ABSTRACT

AMSU-A (Advanced Microwave Sounding Unit-A) measurements for channels that are sensitive to the surface over land have not been widely assimilated into numerical weather prediction (NWP) models due to complicated land surface features. In this paper, the impact of AMSU-A assimilation over land in Southwest Asia is investigated with the Weather Research and Forecasting (WRF) model. Four radiance assimilation experiments with different land-surface schemes are designed, then compared and verified against radiosonde observations and global analyses. Besides the surface emissivity calculated from the emissivity model and surface temperature from the background field in current WRF variational data assimilation (WRF-VAR) system, the surface parameters from the operational Microwave Surface and Precipitation Products System (MSPPS) are introduced to understand the influence of surface parameters on AMSU-A assimilation over land.

The sensitivity of simulated brightness temperatures to different surface configurations shows that using MSPPS surface alternatives significantly improves the simulation with reduced root mean square error (RMSE) and allows more observations to be assimilated. Verifications of 24-h temperature forecasts from experiments against radiosonde observations and National Centers for Environmental Prediction (NCEP) global analyses show that the experiments using MSPPS surface alternatives generate positive impact on forecast temperatures at lower atmospheric layers, especially at 850 hPa. The spatial distribution of RMSE for forecast temperature validation indicates that the experiments using MSPPS surface temperature obviously improve forecast temperatures in the mountain areas. The preliminary study indicates that using proper surface temperature is important when assimilating lower sounding channels of AMSU-A over land.

Key words: AMSU-A, surface temperature, microwave surface emissivity, radiance assimilation

Citation: He Wenying, Liu Zhiquan, and Chen Hongbin, 2011: Influence of surface temperature and emissivity on AMSU-A assimilation over land. *Acta Meteor. Sinica*, **25**(5), 545–557, doi: 10.1007/s13351-011-0501-1.

1. Introduction

The Advance Microwave Sounding Unit-A (AMSU-A) is a cross-track scanning radiometer to measure radiances for 15 channels, of which 12 sounding channels are within the 50–60-GHz oxygen absorption band, and 3 window channels are at 23.8, 31.4, and 89 GHz, respectively. The AMSU-A sounding channels are used for monitoring atmospheric temperature profile and window channels are mainly used for extracting information on surface temperature and emissivity as well as clouds. With high precision and

stability, AMSU-A can provide enhanced information for tropospheric temperature profiles, which is crucial to numerical weather prediction (NWP) systems. One year after AMSU-A launch, the raw AMSU radiance data were assimilated into the ECMWF system and resulted in some useful improvements for analyses and forecasts (McNally et al., 2000). Baker et al. (2005) directly assimilated AMSU-A radiance into the US Navy's operational system and demonstrated the improvement in the model forecast and tropical cyclone track research. To date, AMSU-A measurements have been widely assimilated in numerical forecast models

*Supported by the National Key Basic Research and Development (973) Program of China (2010CB950802 and 2010CB428602) and the National Natural Science Foundation of China (40605011).

†Corresponding author: hwy@mail.iap.ac.cn.

to obtain more accurate estimates of the initial values for the model state variables (Zhao and Wang, 2008). However, AMSU-A assimilation has been more concerned with sounding channels that are not sensitive to the surface, and lower sounding channels have been assimilated over sea only, e.g., channels 4 and 5 are sensitive to lower atmospheric layers and to a lesser extent with surface features. That is because the surface parameters, such as surface temperature and emissivity, are highly variable due to complicated land surface features, which lead to difficulties in assimilating AMSU-A window channels and lower sounding channel observations over land than over sea.

To use AMSU-A observations over land, it requires accurate surface temperature and emissivity. The surface temperatures with high accuracy can be retrieved from satellite measurements, such as the MODIS (Moderate Resolution Imaging Spectroradiometer) land skin temperature product with 0.5-K error (Wan et al., 2002), but it is a challenge to use satellite-retrieved surface temperatures in the NWP model due to different spatial resolutions of satellite instruments. Currently, surface temperature can be forecasted from the NWP model and is usually used as an input for radiance assimilation, though more uncertainties exist for the complex surface features over land.

Surface microwave emissivity is a key factor for AMSU-A assimilation over land. Many methods have been developed to calculate surface emissivity over land. The direct ground-based microwave emissivity measurements have been carried out over different types of land cover (Matzler, 1990, 1994; Wigneron et al., 1997). Due to the spatial and temporal limits of field measurements, satellite observations have been widely used to retrieve land surface microwave emissivity recently (Jones and Vonder Haar, 1997; Ruston and Vonder Haar, 2004; Prigent et al., 1997, 1998; Karbou et al., 2005a, b; He and Chen, 2009). In a different way, Weng et al. (2001) developed a land surface emissivity model for various surface conditions. The emissivity model needs more surface parameters, such as vegetation fraction and land surface temperature, to compute surface emissivity. To use land surface emissivity in the NWP model, Prigent et al. (2005)

directly calculated AMSU-A surface emissivity in the ECMWF system by combining satellite observations and ECMWF background information. Karbou et al. (2006) established three datasets consisting of surface temperature and emissivity retrieved from the satellite measurements for AMSU-A assimilations over land in the Météo-France assimilation system, and evaluated the impact of these assimilations on both analysis and forecast (Karbou et al., 2010a, b). The only land surface emissivity model (Weng et al., 2001) has been integrated into the Community Radiative Transfer Model (CRTM) developed at the US Joint Center for Satellite Data Assimilation (JCSDA) so that direct assimilations of AMSU-A channels that are sensitive to surface are available.

Until now the study of AMSU-A assimilation over land is rather limited due to the complicated surface characteristics of the globe, so we plan to investigate the impact of AMSU-A assimilation over land in a local region. In this paper, the Weather Research and Forecasting (WRF) model provides the regional forecast background, combining with the WRF 3D-VAR assimilation system (Barker et al., 2004) to investigate the impact of the AMSU-A assimilation over land on short-range forecasts in Southwest Asia (SA). Complex topography in SA is dominated with large areas of desert or barren soil and surrounded sea. Many model studies have been implemented in this region and have found that it is difficult to obtain accurate forecast due to its complex topography. Xu et al. (2009) evaluated the WRF model in this region and found that larger model forecast errors occurred in higher mountain areas.

Currently, the CRTM has been applied in the WRF-VAR system (Liu and Barker, 2006; Liu et al., 2009). Considering the complex land surface features in SA and the deficiencies of the land surface emissivity model (Weng, 2007), we introduced the surface parameters derived from the operational Microwave Surface and Precipitation Products System (MSPPS). Gu et al. (2006) used the surface emissivity derived from MSPPS to adjust the surface parameters as input of Weng's emissivity model, and showed the improvements on calculated emissivity. Since both surface

emissivity and land surface temperature (LST) are important for AMSU-A assimilation over land, we plan to integrate the surface emissivity and LST derived from the MSPPS into WRF-VAR system, and to investigate the impact of AMSU-A assimilation over land with different surface configurations on forecasts.

The paper is organized as follows. Section 2 introduces model environments and data. The processing of AMSU-A radiance assimilation in the WRF-VAR system is described in Section 3. The design of experiments is shown in Section 4. Section 5 presents the results of different experiments and verifications against observation and forecasts. Finally, a summary and discussion are given in Section 6.

2. Model and data

The WRF model uses a 45-km grid spacing for the Southwest Asian domain (0–50°N, 0–110°E). The model top is 10 hPa with 57 vertical levels. To assess the impact of radiance assimilation on forecasts, 24-h forecasts are made at 0000, 0600, 1200, and 1800 UTC 23–31 August 2007.

AMSU-A radiance measurements from NOAA-15, NOAA-18, and METOP-2 are directly assimilated into the WRF-VAR system. The 6-h forecast atmospheric states (i.e., temperature and humidity profiles) from the WRF model as the background field provide the input to the CRTM. Surface emissivity is directly calculated from the land microwave emissivity model in CRTM. The inputs for the emissivity model, such as vegetation fraction and land surface temperature, come from the background field.

The operational MSPPS developed by NOAA/NESDIS provides near real-time surface products for AMSU-A. Detailed information is seen at <http://www.star.nesdis.noaa.gov/corp/scsb/mspps/>. AMSU-A land surface temperature and emissivity at 23.8, 31.4, and 50.3 GHz are derived from their brightness temperature in the MSPPS algorithm (details refer to the MSPPS Users' Manual). To obtain more accurate surface temperature, the screening procedures are applied to remove precipitation, snow-cover, and wetness area. The retrieved land surface emissivity is

difficult to validate due to the lack of direct emissivity measurements while the retrieved land surface temperature is validated with the sheltered air temperature observations (at 2-m height) from surface weather stations. Both temperatures are consistent with a high coefficient of 0.96. Although surface temperature is not strictly the same as air temperature at 2-m height, their high consistency indicates the reliability of the MSPPS land surface temperature.

To directly use the MSPPS surface temperature and emissivity in WRF-VAR system, their retrieval algorithms are added into the program of WRF-VAR. The screening procedures for MSPPS surface temperature are also added into the quality control (QC) part of WRF-VAR system in this study. The QC issues are introduced in the next section.

3. AMSU-A radiance assimilation in WRF-VAR

A brief introduction of AMSU-A radiance assimilation in WRF-VAR system is given here.

3.1 Channel selection

Similar to previous studies, channels (1–4, 15) that are sensitive to land surface are not used, and sounding channels 10–14 above model top are not used either. Thus, sounding channels 5–9 that are sensitive to tropospheric and lower stratospheric temperature are assimilated in the current WRF-VAR system.

3.2 Bias correction

The systematic differences between observed and simulated radiances arise mainly from the deficiency in radiative transfer model, instrument problems or biases in the model fields. Those biases can be significant and must be removed before assimilation. In this study, the bias parameters are estimated within the variational assimilation, and join with the atmospheric model state, which is called variational bias correction (VarBC) (Dee, 2005; Auligne et al., 2007). Bias correction coefficients estimated from current assimilation cycle will be used as the background for the next assimilation cycle.

3.3 Quality control

There are specific quality controls for different sensors in WRF-VAR system. Here, AMSU-A measurements over sea are removed since we are concerned about AMSU-A assimilation over land. For 30 scan positions of AMSU-A, the radiances at the scan positions 1–3 and 28–30 are not used due to the limb effect of observations. In addition, the screen procedures for precipitation, snow-cover and wet area referred to the MSPPS algorithms are used in quality control. The final quality control eliminates those innovations (observed minus background after bias correction) which are greater than 15 K or exceed three times the given observation error standard deviation.

4. Experimental design

Previous studies (Karbou et al., 2006) show that the various surface setting should not be ignored, even for the sounding channels of AMSU-A. Since AMSU-A channels 4 and 5 are sensitive to the lower atmosphere and to a lesser extent with surface features, we focus on the surface alternatives for channels 4 and 5 here.

To use alternatives, the surface temperature and land surface emissivity are firstly derived from the MSPPS retrieval algorithm, and then replace the corresponding surface temperature derived from the background field and emissivity calculated from CRTM. In MSPPS algorithms, the surface temperature and emissivity of AMSU-A channels 1–3 are calculated us-

ing their brightness temperatures, so the three window channels are not assimilated. The MSPPS surface temperatures are used for the remaining sounding channels. The emissivity of AMSU-A channel 5 is derived from the MSPPS surface emissivities of channels 1–3 using frequency extrapolation due to the smooth variation of emissivity with frequency (Farbou et al., 2005a). No emissivity modification is made for sounding channels 6–9 because of the negligible influence of surface emissivity.

Therefore, five assimilation experiments are designed as listed in Table 1. The first one, called GTS hereafter, only assimilates the conventional observations from the Global Telecommunication System (GTS) in the WRF-VAR system to differ from the others with AMSU-A radiance assimilation. The other four experiments assimilate both GTS observations and AMSU-A radiance measurements, but using different land-surface schemes. The second experiment, GS59, is the default AMSU-A radiance assimilation scheme in the current WRF-VAR system, which assimilates AMSU-A sounding channels 5–9, and uses the surface temperature from background field and the emissivity calculated from CRTM. In the third and fourth experiments, only the surface temperature alternative is used. The alternatives of both surface temperature and emissivity of channel 5 are used in the fifth experiment. To study the influence of lower channels, the fourth experiment assimilates sounding channels 4–9.

Table 1. Experiments designed with different assimilated observations and land-surface schemes

Name	Assimilated observations	Surface temperature (Ts)	Emissivity (EM)
GTS	GTS		
GS59	GTS+AMSUA-S5-9	First guess	CRTMch5-9
GS59_Ts		MSPPS	CRTMch5-9
GS49_Ts	GTS+AMSUA-S4-9	MSPPS	CRTMch4-9
GS59_Ts+em5	GTS+AMSUA-S5-9	MSPPS	MSPPSch5+CRTMch6-9

5. Results and verifications

5.1 Sensitivity of brightness temperature to surface configurations

To see the influence of different land surface schemes, firstly the difference between simu-

lated and observed brightness temperature at channel 5 for radiance experiments is investigated. Due to the same surface configuration at channel 5 in GS59_Ts and GS49_Ts, the brightness temperature differences among experiments GS59, GS59_Ts, and GS59_Ts+em5 are compared.

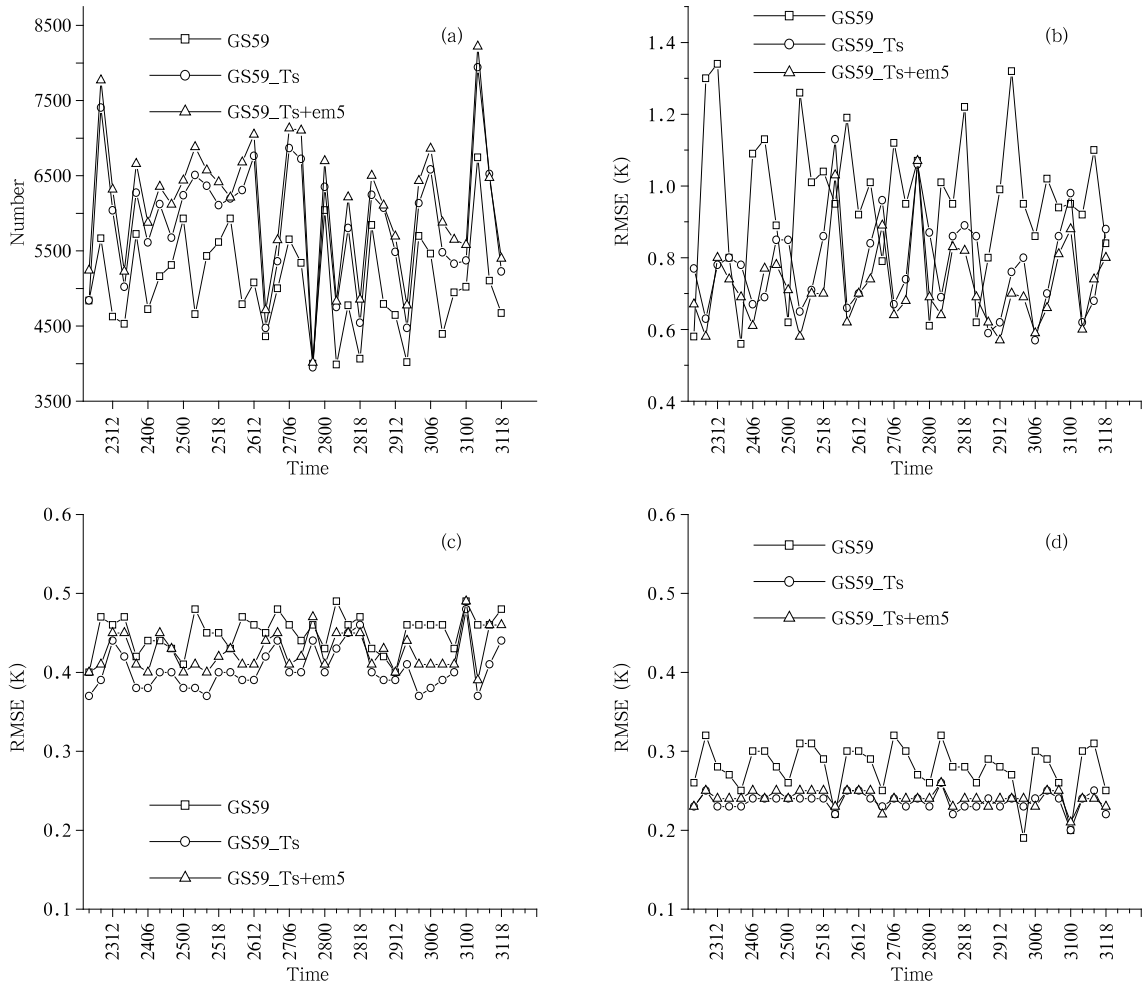


Fig. 1. Variations of observation number (a) and difference of brightness temperature before (b) and after (c) bias correction and after analysis (d) in three radiance experiments. The period is from 0000 UTC 23 to 1800 UTC 31 August 2007.

Figure 1a shows the variations of the observation numbers used in the three assimilation experiments. The default scheme GS59 uses the least observation numbers, and the new schemes using surface alternatives make more than 500–2000 observations available, which demonstrates that more qualified observations can be used in the new schemes. For the new schemes using surface alternative, the observation number in GS59_Ts+em5 is higher about 100–300 than GS59_Ts, and their variation trend is consistent. Therefore, the large number difference between GS59 and new schemes is mainly caused by using surface temperature alternative rather than using surface emissivity alternative, although the surface emissivity

also generates weak positive impact on channel 5.

We further use root mean square error (RMSE) to describe the variation of simulated and observed brightness temperature in each scheme. The definition of RMSE is seen in Eq. (1):

$$\text{RMSE} = \sqrt{\frac{1}{N} \sum_{i=1}^N (X_s - X_{\text{obs}})^2}, \quad (1)$$

where X_s and X_{obs} stand for simulated and observed brightness temperature (Tb), respectively. RMSE of Tb before/after bias correction is shown in Figs. 1b and 1c, respectively, and RMSE of Tb after analysis is shown in Fig. 1d. The biases of observed and

calculated Tb mostly depend on both scan angle and air mass, and need to be corrected before data enter into minimization procedure. The bias correction scheme based on simple linear regression is adopted in current WRF-VAR system, detailed description referred to Liu and Barker (2006).

Without bias correction, Fig. 1b shows large RMSE in the three radiance schemes. In particular, the RMSE in the GS59 scheme shows a large variation range with time, such as 0.6 K at 0000 UTC and 1.4 K at 1200 UTC in a day. Among the three schemes, RMSEs for the new schemes using surface alternatives, GS59_Ts and GS59_Ts+em5, are much smaller than that for GS59, which shows the positive impact on simulated Tb when using surface alternatives. The variations of RMSE with time for the new schemes are quite similar, but RMSE of GS59_Ts+em5 is even smaller than that of GS59_Ts, which infers that using both alternatives is better than using single one although the second one might have less contribution. Combined with the numbers in Fig. 1a, it is seen that using MSPPS surface alternatives can significantly improve the simulated Tb, and the contribution of surface temperature is more obvious than that of surface emissivity at channel 5.

After bias correction, the differences of RMSE among the schemes become smaller, and the variation range of RMSE mostly changes from 0.4 to 0.5 K (Fig. 1c)—unlike the RMSE before bias correction changes from 0.6 to 1.4 K (Fig. 1b), which shows the strong effect of bias correction.

Beside the simulated Tb, also called background radiance, the analysis Tb can be generated using increments to adjust the background radiance to observation as close as possible. Therefore, the RMSE between observed and analysis Tb in Fig. 1d is smaller than those in Figs. 1b and 1c, changing from 0.2 to 0.3 K. After analysis, the RMSE for the schemes using surface alternatives is more constant, around 0.25 K, while the RMSE for the default radiance scheme appears a relatively large variation range with time.

The comparisons of observation number and RMSE of Tb among the three experiments show that using surface alternatives can improve the simulated

Tb and allow more observations used for assimilation. For the two surface alternatives schemes, using the surface temperature alternative shows more obvious impact on simulated Tb than using the surface emissivity alternative for channel 5, which indicates that radiance at channel 5 is more sensitive to surface temperature than surface emissivity.

5.2 Verifications

Since AMSU-A is mainly used for measuring atmospheric temperature, especially as channels 4 and 5 are more sensitive to lower atmosphere, the forecast temperature from the assimilation experiments is verified against the observations and NCEP global analyses to investigate the influence of AMSU-A assimilation over land. The 24-h forecasts are generated at 0000, 0600, 1200, and 1800 UTC from 23 to 31 August 2007.

5.2.1 Verification against radiosonde observations

Temperature forecasts from the assimilation experiments are verified against radiosonde observations. The period is about 1 week from 0000 UTC 24 to 1800 UTC 31 August. The validation is made at 0000 and 1200 UTC due to fewer radiosonde observations at 0600 and 1800 UTC. The RMSE of temperature difference between forecast and observation is used to describe the difference of experiments.

Figure 2 shows the verification of temperature profiles for 6- and 12-h forecast of 5 experiments. For 6-h forecast (Fig. 2a), the new schemes using surface alternatives show more positive impact on temperature below 700 hPa than the scheme only assimilating GTS, such as obviously reduced RMSE at 850 hPa, while GS59 shows a slight negative effect, compared to GTS, at lower atmospheric layers. Since these schemes focus on changing surface temperature and emissivity for channels 4 and 5, which are more sensitive to lower atmosphere, the improved temperature forecast below 700 hPa is mostly likely attributed to the MSPPS land surface parameters. As to 12-h forecast (Fig. 2b), the positive effect of new schemes is slight at lower atmosphere, and it is not so clear as the 6-h forecast to show the difference among experiments.

To see more detail for the temperature forecasts

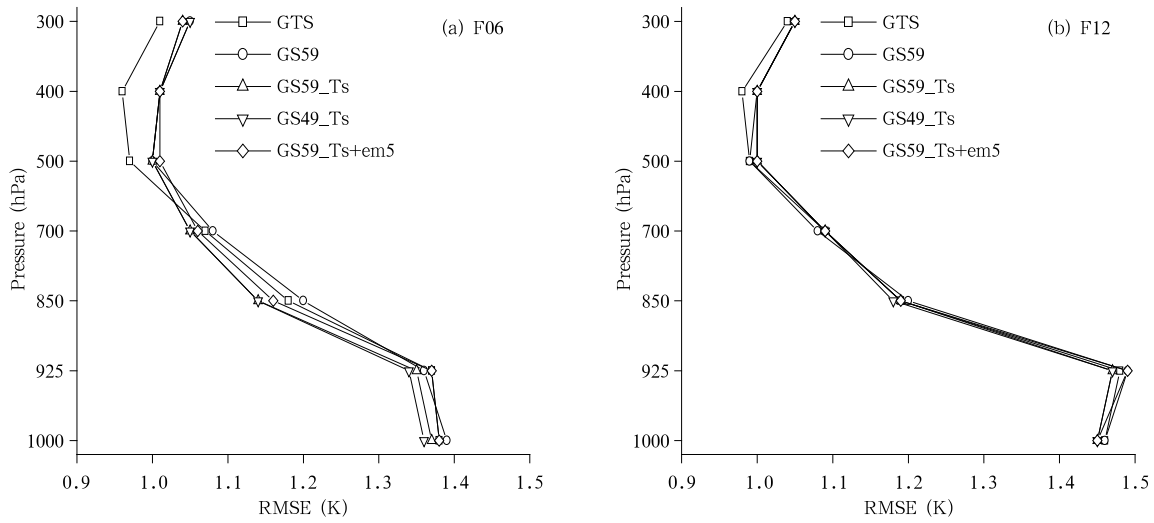


Fig. 2. Verification of forecast temperature profile of experiments against radiosonde observations at 0000 and 1200 UTC 24–31 August 2007. (a) 6-h forecast and (b) 12-h forecast.

at lower layers of atmosphere, the validations of the 24-h forecast temperature at 850 and 700 hPa are made at 0000 and 1200 UTC. The RMSE shown in Fig. 3 increases with forecast time, and the influences of different experiments are obvious at 6- and 18-h forecast, especially at 850 hPa, while the influences are weak at 12-h forecast. Among these experiments, the GTS shows larger RMSE with increasing forecast range, especially 18- and 24-h forecast. The default radiance scheme GS59 mostly shows larger RMSEs for 6-, 12-, and 18-h forecast. The new schemes using surface alternatives generally show smaller RMSE at four forecast times and their RMSEs are close. Relatively,

GS49_Ts shows the smallest RMSE for 6-, 12-, and 18-h forecast at 850 hPa. In general, the new schemes using surface alternatives show more positive impact on forecast temperature than the default radiance scheme and the only GTS assimilation scheme within 24-h forecast at the three pressure levels. Among the three new schemes, the scheme assimilating sounding channels 4–9 and using surface temperature alternative seems optimal, and the other two schemes assimilating sounding channels 5–9 present similar but slightly less positive impact on forecast temperature.

Figure 4 shows the time series of 6- and 12-h forecast temperature verification at 850 hPa within one

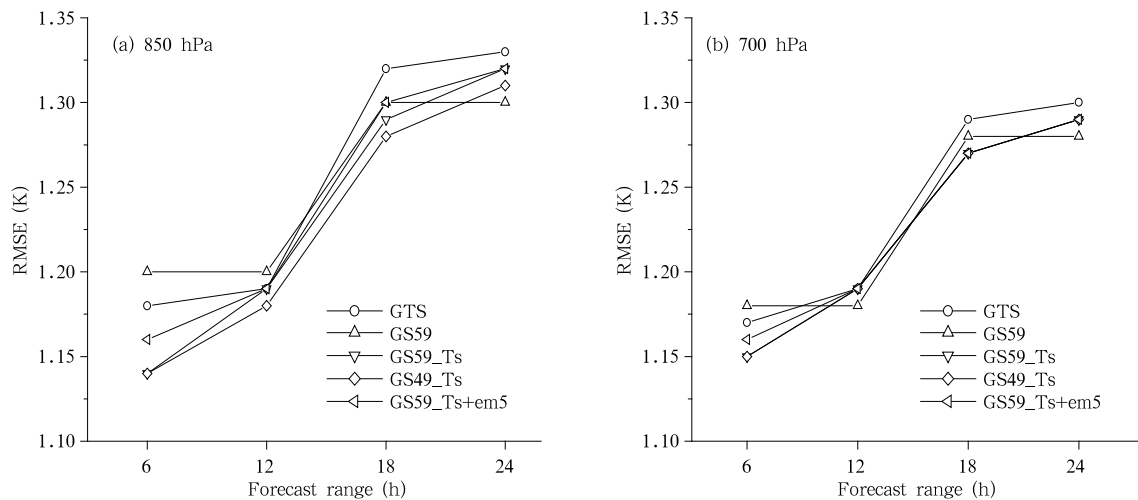


Fig. 3. Verification of temperature forecast at (a) 850 hPa and (b) 700 hPa against radiosonde observations.

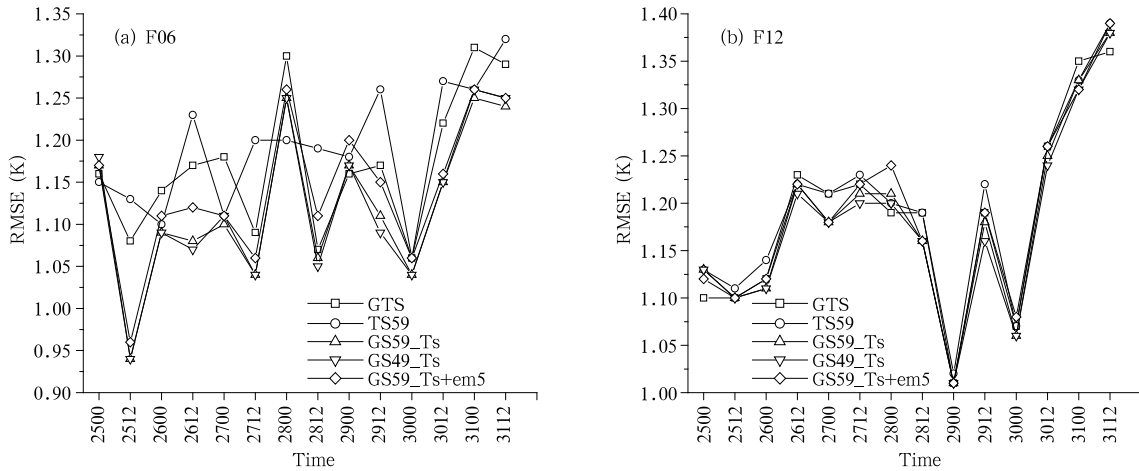


Fig. 4. Time series of (a) 6-h and (b) 12-h forecast temperature verification against radiosonde at 850 hPa.

week. For 6-h forecast validation as shown in Fig. 4a, five experiments show obviously different influences at 0000 and 1200 UTC. Relatively, their RMSEs are closer at 0000 UTC but quite different at 1200 UTC. At 1200 UTC, the default radiance scheme, GS59, mostly shows the largest RMSE, and the new schemes using surface alternatives show lower and closer RMSE. The variation range of RMSE among experiments is about 0.2 K at 1200 UTC while it is less than 0.05 K at 0000 UTC. It infers that the improvements occurred in the new schemes for 6-h forecast validation in Fig. 3 mainly attribute to their clearly reduced RMSE in validation made at 1200 UTC rather than 0000 UTC of each day.

Different from 6-h forecast, the different influences on 12-h forecast temperature (Fig. 4b) are slight. Their RMSEs are close at both 0000 and 1200 UTC, and their differences in RMSE are mostly less than 0.05 K. The variation trend of RMSE for 18-h forecast (figure omitted) is similar to that for 6-h forecast, with larger differences occurring at 1200 UTC especially. For 24-h forecast (figure omitted), the influence of those experiments seems similar and changes more consistently with time. The obvious differences of the 6- and 18-h forecast verifications made at 1200 UTC imply that assimilation experiments have a strong influence on temperature forecasts initialized from 0600 and 1800 UTC, and particularly, the new schemes show more positive impacts.

5.2.2 Verification against NCEP global analyses

To verify the forecast temperature from assimilation experiments against NCEP global analyses, global

fields are interpolated into the Southwest Asian domain and the corresponding resolution used in WRF model.

First, the time series of RMSEs for 6- and 12-h forecast temperature verification against NCEP global analyses at 850 hPa within one week are shown in Fig. 5. Different from verification against radiosonde, RMSEs for five experiments show regular wave variation at 0000 and 1200 UTC. The RMSE at 0000 UTC is much lower than that at 1200 UTC, and especially RMSE difference between 0000 and 1200 UTC is 0.2–0.4 K for 6- and 12-h forecast validations. The influences of experiments on forecast temperature are more different at 1200 UTC rather than at 0000 UTC. When validation made at 1200 UTC, for 6-h forecast, GS95 shows the largest RMSE and GS95_Ts_em5 using both alternatives shows the least RMSE to cause about 0.1–0.2-K difference; while for 12-h forecast, RMSEs of the four radiance assimilation experiments are quite close and about 0.1 K lower than that of GTS.

Due to the obviously different validation results at 1200 UTC for experiments, we compare the overall 24-h forecast temperature validation made at 1200 UTC for experiments. Figure 6a shows the RMSE difference among five experiments at 850 hPa within 24-h forecast. For 6-h forecast, RMSEs of the new schemes are smaller than that of GTS and GS59. For 12- and 18-h forecast, RMSE of GTS is much larger than that of four radiance schemes, and those radiance schemes show similar influences for longer forecast. The variation of RMSE at 700 hPa (Fig. 6b) is similar to that at 850 hPa. For 6-h forecast, RMSE of the default

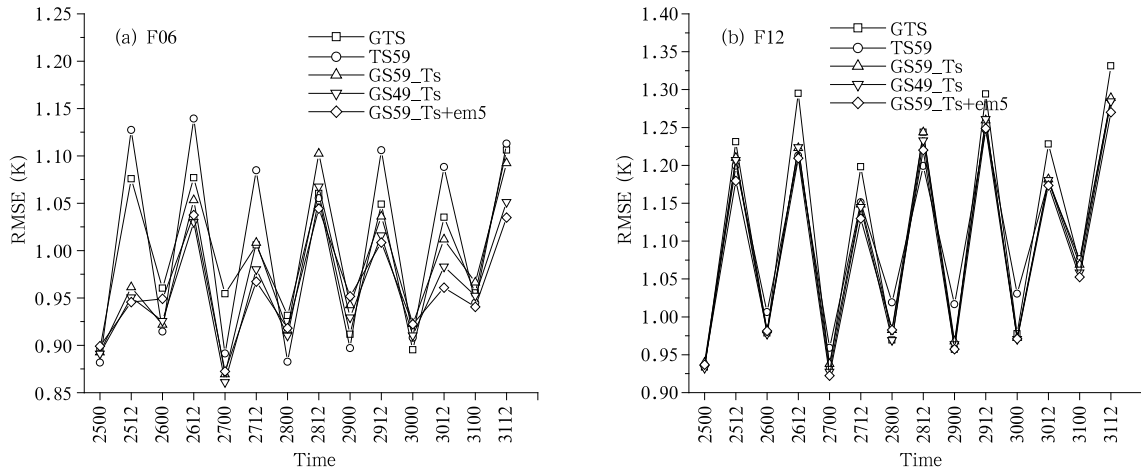


Fig. 5. Time series of (a) 6-h and (b) 12-h forecast temperature verification against NCEP global analyses at 850 hPa.

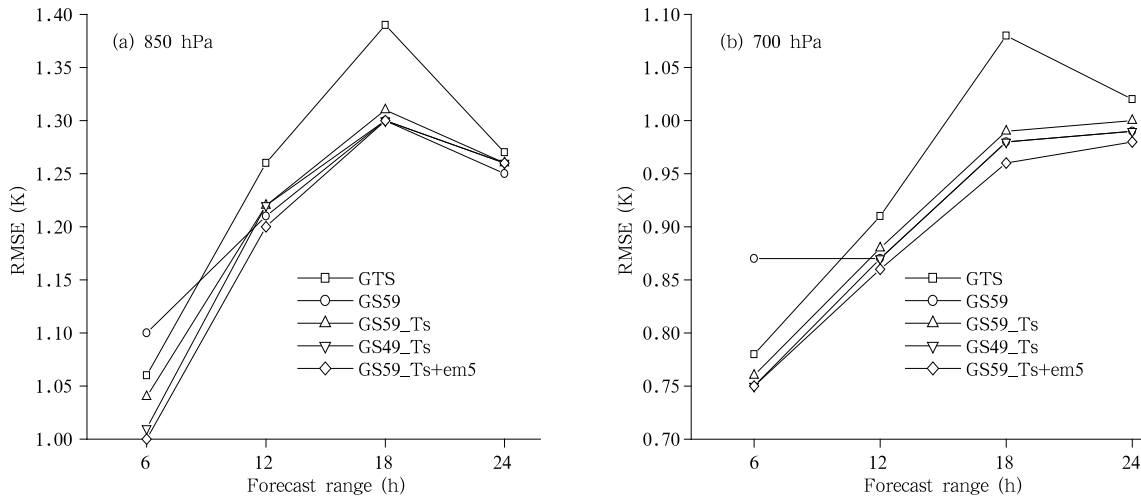


Fig. 6. Temperature verification at (a) 850 and (b) 700 hPa against NCEP global analyses.

radiance assimilation scheme is larger than that of other schemes; in particular, the former is larger about 0.1 K than the latter. With a longer forecast range, RMSE of GTS increases rapidly from 0.75 K for 6-h forecast to 1.1 K for 18-h forecast. Relatively, the RMSEs of experiments at 700 hPa are much smaller than the corresponding values at 850 hPa. Among the three new schemes, the GS59_Ts+em5 using both surface alternatives shows the smallest RMSE within 24-h forecast, especially at 700 hPa, which implies that using both surface alternatives is better than using only surface temperature alternative although the contribution of surface emissivity is small.

In general, the verifications against the NCEP

global analyses show that the new schemes using surface alternatives produce positive impact on temperature forecasts, especially for 6-h forecast, and assimilating conventional observations and AMSU-A radiance together show more obviously positive influence than only assimilating GTS for longer forecast range, such as 18-h forecast.

The spatial distribution of RMSE for assimilation experiments in this domain is further investigated. Here, three experiments, GTS, GS59, and GS59_Ts+em5, are used to stand for no radiance, default radiance, and new radiance assimilation schemes. Since a more obvious RMSE difference occurred for 6- and 18-h forecast validation at 1200 UTC in Fig. 6,

the spatial distribution of RMSE of 6- and 18-h forecast verification against the NCEP global analyses at 850 hPa calculated at 1200 UTC is shown in Fig. 7. For 6-h forecast, a distinctive RMSE difference occurs

in the black circle area, which is the tail of Tibetan Plateau and mostly dominated by desert or barren soil. Among the three experiments, GTS shows a large RMSE of about 2–3 K in part of the black circle area,

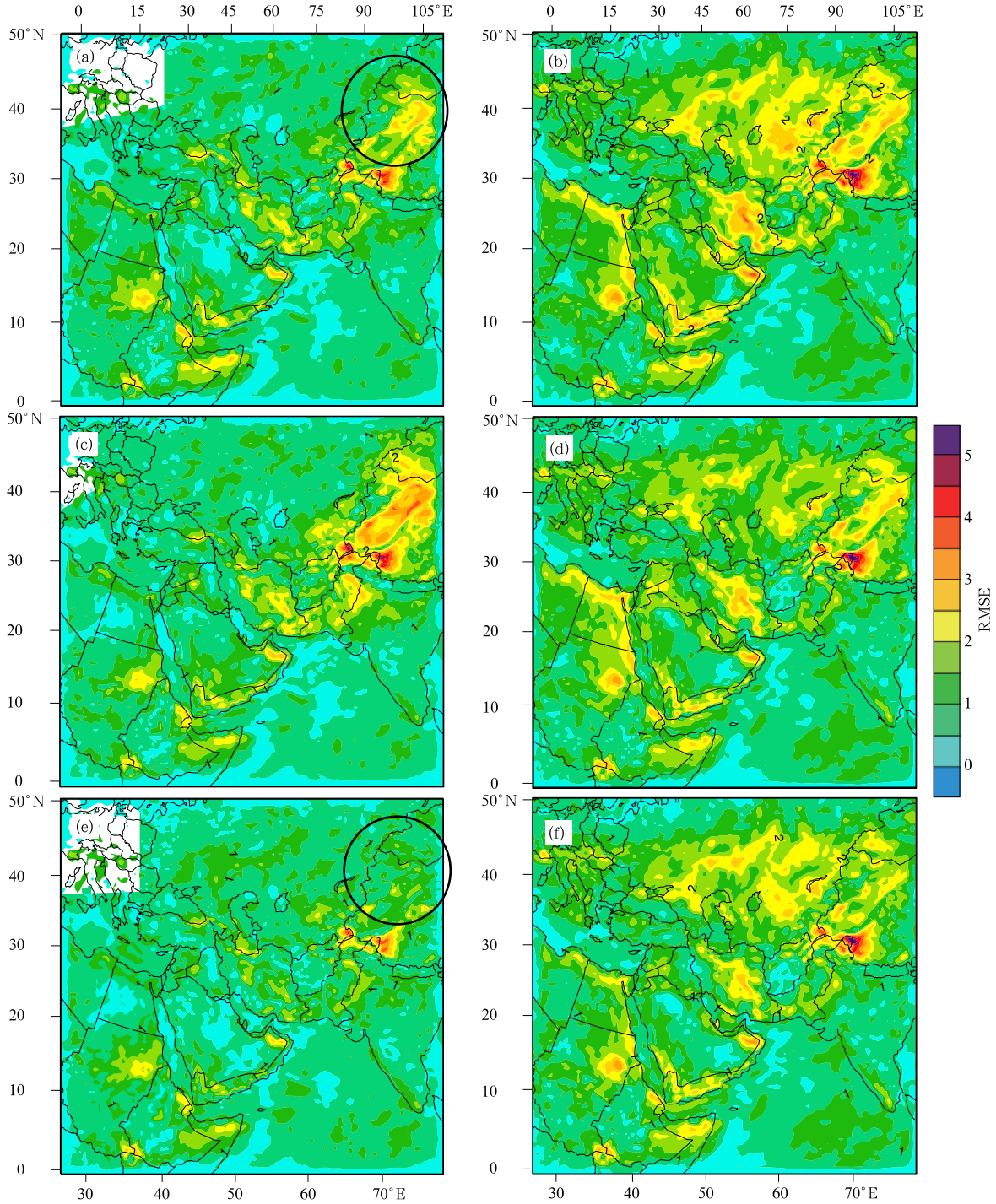


Fig. 7. Distribution of RMSE for 6-h (left panels) and 18-h (right panels) forecast temperature verification against NCEP global analyses at 850 hPa over Southeast Asia. Three experiments from up to down are GTS, GS59, and GS59-Ts+em5, respectively.

and the default scheme, GS59, shows a larger RMSE of about 2.5–3.5 K in most of this area; but the new scheme, GS59_Ts+em5, using both surface temperature and emissivity alternatives, shows small RMSE of about 1–1.5 K in this area. In the recent study by Xu et al. (2009) over Southwest Asia, they pointed out that the largest model error occurred in the highest terrain region, the Himalayan Mountain range, due to a model deficit in the description of surface temperature in high terrain areas. Therefore, the reduced RMSE of the new scheme in the mountain area indicates that the surface temperature from MSPPS is more reasonable than that from the background field generated from model forecast. Besides the distinctive difference in the black circle area, in the middle of this domain, the RMSE of the new scheme is also smaller than those of GTS and GS59.

The spatial distribution of RMSE helps understand why the new schemes show more positive influence on 6-h forecast temperature and where those positive influences come from. As to the remarkable improvement occurring in the black circle area, we must combine the detail land surface feature of this area to figure out the differences. The right panels in Fig. 7 are for 18-h forecast temperature verification. With longer forecast time, the RMSE for GTS seems much larger than that for both radiance assimilation schemes for high latitude area, such as over 30°N, so that the averaged RMSE of GTS for 18-h forecast is larger than that of those radiance assimilation schemes as shown in Fig. 6a. Similarly, the new radiance scheme shows smaller RMSE than the default radiance scheme in the black circle area but larger RMSE in the upper-middle part of the domain, so the averaged influences of both radiance assimilation schemes are similar, as shown in Fig. 6a.

6. Summary and discussion

In this paper, the impact of AMSU-A assimilation over land in the WRF model is investigated in Southwest Asia. We design radiance assimilation experiments using different surface temperature and emissiv-

ity for AMSU-A sounding channels 4 and 5, which are sensitive to surface. The influences of AMSU-A assimilation over land with different surface configurations are analyzed by comparing and validating their temperature forecasts with observations and global analyses.

The sensitivity of brightness temperature to those surface configurations shows that using the MSPPS-retrieved surface temperature can significantly improve the simulated radiance so that more observations are allowed to be assimilated. Relatively, using emissivity alternative for channel 5 generates less positive influence on simulated radiance.

To understand the impact of AMSU-A assimilation over land with different surface configurations on forecast, the 24-h forecast temperature from assimilation experiments is verified against radiosonde observations and NCEP global analyses. The new assimilation schemes using surface alternatives show positive impact on temperature forecasts at lower atmospheric layers, especially at 850 and 700 hPa. The spatial distribution of RMSE for forecast temperature validation in this domain shows that new radiance schemes using surface alternatives generate much improvement for 6- and 18-h forecast over the mountain areas surrounded by desert. Model evaluations in Southwest Asia by Xu et al. (2009) show that the largest model error occurred in western Himalayan Mountain due to the model deficiencies in the description of surface temperature in high terrain areas. The obvious difference in high altitude area further demonstrates that the surface temperature from the MSPPS is more reasonable than that from background forecast field.

The one-week study of AMSU-A assimilations over land in Southwest Asia shows positive influence on forecast. The results indicate that using proper surface temperature is more important to improve radiance and forecast temperature when assimilating AMSU-A lower sounding channels. The promising results in this paper need more long-term analysis and validation, and the surface temperature and emissivity derived from other measurements would be further explored for radiance assimilation in NWP to assess

the impact of surface parameters on AMSU-A assimilation over land.

Acknowledgments. The authors thank NCAR/MMM staff, especially Hui-Chuan Lin and Craig Schwartz.

REFERENCES

- Auligne, T., A. McNally, and D. Dee, 2007: Adaptive bias correction for satellite data in a numerical weather prediction system. *Quart. J. Roy. Meteor. Soc.*, **133**, 631–642.
- Baker, N. L., T. F. Hogan, W. F. Campbell, R. L. Pauley, and S. D. Swadley, 2005: The impact of AMSU-A radiance assimilation in the U. S. Navy's Operational Global Atmospheric Prediction System (NOGAPS), NRL Memorandum Report Memo. Rep. (NRL/MR/7530-05-8836), 18pp Naval Res. Lab., Monterey, CA, 93943–5502.
- Barker, D. M., W. Huang, Y.-R. Guo, A. J. Bourgeois, and Q. N. Xiao, 2004: A three-dimensional variational data assimilation system for MM5: Implementation and initial results. *Mon. Wea. Rev.*, **132**, 897–914.
- Dee, D. P., 2005: Bias and data assimilation. *Quart. J. Roy. Meteor. Soc.*, **131**, 3323–3343.
- He Wenying and Chen Hongbin, 2009: The characteristics of microwave land emissivity over Chinese Jianghuai-Huanghuai Region. *Remote Sens. Tech. Appl.*, **24**, 297–303. (in Chinese)
- Gu Songqiang, Wang Zhenhui, Weng Fuzhong, Xue Jishan, and Dong Peiming, 2006: A study for improving microwave land surface emissivity model with NOAA/AMSU data and the GRAPES 3DVar system. *Plateau Meteorology*, **25**, 1101–1106. (in Chinese)
- Jones, A. S., and T. H. Vonder Haar, 1997: Retrieval of microwave surface emittance over land using coincident microwave and infrared satellite measurements. *J. Geophys. Res.*, **102**, D12, 13609–13626/299–310.
- Karbou, F., C. Prigent, L. Eymard, and J. R. Pardo, 2005a: Microwave land emissivity calculations using AMSU measurements. *IEEE Trans. Geosci. Rem. Sensing*, **43**, 948–959.
- , and —, 2005b: Calculation of microwave land surface emissivities from satellite observations: Validity of the specular approximation over snow-free surfaces. *IEEE Trans. Geosci. Remote Sensing Letts.*, **2**, 311–314.
- , E. Gérard, and F. Rabier, 2006: Microwave land emissivity and skin temperature for AMSU-A and -B assimilation over land. *Quart. J. Roy. Meteor. Soc.*, **132**, 2333–2355.
- , —, and —, 2010a: Global 4DVAR assimilation and forecast experiments using AMSU observations over land. Part I: Impacts of various land surface emissivity parameterizations. *Wea. Forecasting*, **25**, 5–19.
- , F. Rabier, J. -P. Lafore, J. -L. Redelsperger, and O. Bock, 2010b: Global 4DVAR assimilation and forecast experiments using AMSU observations over land. Part II: Impacts of assimilating surface-sensitive channels on the African monsoon during AMMA. *Wea. Forecasting*, **25**, 20–36.
- Liu Z.-Q., X. Zhang, T. Auligne, and H. -C. Lin, 2009: Variational Analysis of Hydrometeors with Satellite Radiance Observations: A Simulated Study. 10th WRF Users Workshop, June 23–26, 2009, Boulder, Colorado.
- , and D. M. Barker, 2006: Radiance Assimilation in WRF-Var: Implementation and Initial Results. 7th WRF Users Workshop, June 19–22, 2006, Boulder, Colorado.
- Matzler, 1990: Seasonal evolution of microwave radiation from an oat field. *Remote Sens. Environ.*, **31**, 161–173.
- , 1994: Passive microwave signatures of landscapes in winter. *Meteor. Atmos. Phys.*, **54**, 241–260.
- McNally A. P., J. C. Derber, W. -S. Wu, and B. B. Katz, 2000: The use of TOVS level-1B radiances in the NCEP SSI analysis system. *Quart. J. Roy. Meteor. Soc.*, **126**, 689–724.
- Prigent, C., W. B. Rossow, and E. Matthews, 1997: Microwave land surface emissivities estimated from SSM/I observations. *J. Geophys. Res.*, **102**, 21867–21890.
- , —, and —, 1998: Global maps of microwave land surface emissivities: Potential for land surface characterization. *Radio Sci.*, **33**, 745–751.
- , F. Chevallier, F. Karbou, P. Bauer, and G. Kelly, 2005: AMSU-A land surface emissivity estimation for numerical weather prediction assimilation schemes. *J. Appl. Meteor.*, **44**, 416–426.
- Ruston R. C., and T. H. Vonder Haar, 2004: Characterization of summertime microwave emissivity from the Special Sensor Microwave Imager over the conterminous United States. *J. Geophys. Res.*, **109**, D19103, doi:10.1029/2004JD004890.

- Wan, Z., Y. Zhang, R. Wang, and Z. -L. Li, 2002: Validation of the land-surface temperature products retrieved from Terra Moderate Resolution Imaging Spectroradiometer data. *Remote Sens. Environ.*, **83**, 163–180.
- Weng, F., 2007: Advances in radiative transfer modeling in support of satellite data assimilation. *J. Atmos. Sci.*, **64**, 3803–3811.
- , B. Yan, and N. C. Grody, 2001: A microwave land emissivity model. *J. Geophys. Res.*, **106**, 20115–20123.
- Wigneron, J. -P., D. Guyon, J. -C. Calvet, G. Courrier, and N. Bruignier, 1997: Monitoring coniferous forest characteristics using a multifrequency microwave radiometry. *Remote Sens. Environ.*, **60**, 299–310.
- Xu J., S. Rugg, L. Byerle, and Z. Liu, 2009: Weather forecasts by the WRF-ARW model with the GSI data assimilation system in the complex terrain areas of Southwest Asia. *Wea. Forecasting*, **24**, 987–1008.
- Zhao Y., and B. Wang, 2008: Numerical experiments for Typhoon Dan incorporating AMSU-A retrieved data with 3DVM. *Adv. Atmos. Sci.*, **25**, 692–703.